Supporting Information

High Hole Mobility and Efficient Ambipolar Charge Transport in Heterocoronene-based Ordered Columnar Discotics

Joydip De,[†] Indu Bala,[†] Santosh Prasad Gupta,[‡] Upendra Kumar Pandey,[#$*] and Santanu Kumar Pal[†*]

[†]*Department of Chemical Sciences, Indian Institute of Science Education and Research (IISER) Mohali, Sector-81, SAS. Nagar, Knowledge City, Manauli-140306, India*
[‡] *Department of Physics, Patna University, Patna-800005, India*
[#] *Interdisciplinary Centre for Energy Research (ICER), Indian Institute of Science (IISc) Bangalore, C. V. Raman Road, Bangalore 560012, Karnataka, India.*

[$] *Present Address: Department of Electrical Engineering, School of Engineering, Shiv Nadar University, Gautam Buddha Nagar, Uttar Pradesh- 201314, India*

E-mail: skpal@iisermohali.ac.in, santanupal.20@gmail.com, upendra.pandey@snu.edu.in

Table of contents		
S. No.	**Contents**	**Page No.**
1	Experimental section, synthesis and characterization details	S3-S6
2	NMR spectra	S7-S9
3	TGA data	S10
4	DSC data	S10
5	POM data	S11
6	X-ray data	S11-S15
7	Photo-physical studies	S16
8	Electrochemical studies	S17
9	Computational studies	S18
10	SCLC measurements	S19-S26

1) Experimental Section

Materials. Chemicals and solvents (AR quality) were used as received without any further purification. Column chromatographic separations were performed on silica gel (100–200 & 230-400 mesh). Thin layer chromatography (TLC) was performed on aluminium sheets pre-coated with silica gel (Merck, Kieselgel 60, F254).

Measurements and Characterizations. The synthesized materials were structurally characterized by combining the spectroscopic techniques as reported elsewhere.[1] The characterization details have been reproduced for convenience to the readers.[1] Briefly the details are the following. "Structural characterization of the compounds was carried out through a combination of infrared spectroscopy (IR) (Perkin Elmer Spectrum Two), ^{1}H NMR and ^{13}C NMR (Bruker Biospin Switzerland Avance-iii 400 MHz and 100 MHz spectrometers respectively), UV-vis-NIR spectrophotometers (Agilent Technologies, Cary 5000) and Mass spectrometry (Water Synapt G-2-s QTOF with MALDI ion source and α-cyano-4-hydroxy-cinnamic acid as a matrix). IR spectra were recorded in neat form for target compounds. ^{1}H & ^{13}C NMR spectra were recorded using deuterated chloroform ($CDCl_3$) as solvent and tetramethylsilane (TMS) as an internal standard. Cyclic Voltammetry (CV) experiments were performed by using Princeton Applied Research VersaSTAT 3. The transition temperatures and associated enthalpy values were determined using a differential scanning calorimeter (Perkin Elmer DSC 8000 coupled to a controlled liquid nitrogen accessory (CLN 2)) which was operated at a scanning rate of 10 °C min^{-1} both on heating and cooling. Thermogravimetric analysis (TGA) was carried out from 25 to 500 °C (at a heating rate of 10 °C min^{-1}) under nitrogen atmosphere on a Shimadzu DTG-60 instrument. Textural observations of the mesophase were performed with Nikon Eclipse LV100POL polarizing optical microscope (POM) provided with a Linkam heating stage (LTS 420). All images were captured using a Q-imaging camera. X-ray diffraction (XRD) was carried out by filling samples in glass capillaries using Cu-K_α (λ = 1.5418 Å) radiation from Xeuss (Model C HP100 fm) X-ray diffractometer from Xenocs equipped with GeniX 3D source operating at 50 kV and 0.6 mA in conjunction with a multilayer mirror and Pilatus 200 hybrid pixel detector from Dectris. For space charge limited current (SCLC) measurement cell thickness of the samples were measured by using interferometry (Perkin Elmer lambda 35). Current -Voltage measurement and dielectric constant of the samples were measured using Keithley 4200 SCS parametric analyzer."

Synthesis and characterization details:

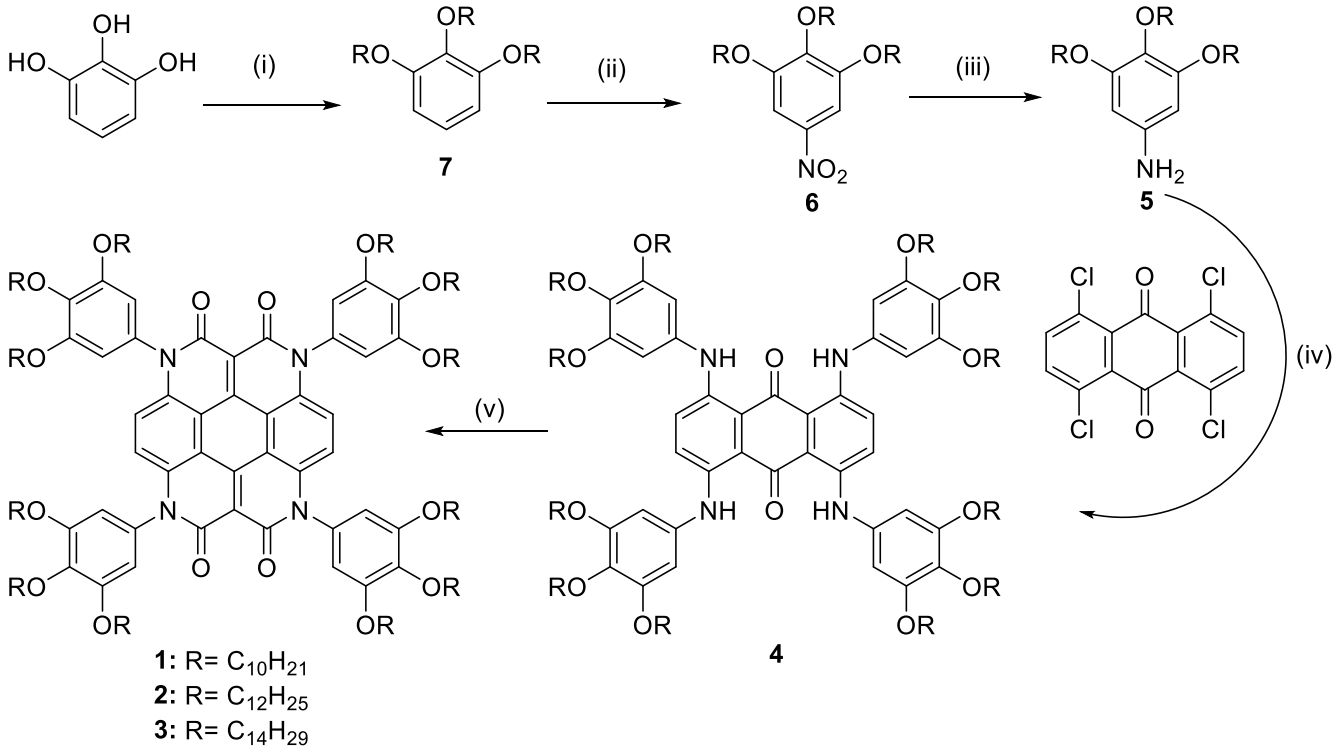

Scheme S1. Synthesis of heterocoronene derivatives **1-3**. Reagents and Conditions: (i) K_2CO_3, alkyl bromide, acetone, 56 °C, 18h; (ii) $NaNO_2$, Conc. HNO_3, DCM, RT, 12h; (iii) Pd-C, dry THF, 24h; (iv) $Pd_2(dba)_3$, BINAP, Cs_2CO_3, toluene, 105 °C, 48 h; (v) CH_3COOK, DMF, diethyl malonate, microwave, 170 °C, 2h.

Experimental Procedure:

Synthesis:

Procedure for the synthesis of 4:

1,4,5,8-tetrachloro-9,10-anthracenedione (1 equiv.), 3,4,5-tris(alkoxoxy)aniline[2] (**5**) (7 equiv.) and Cs_2CO_3 (12 equiv.) were dissolved in 50 ml dry toluene under nitrogen atmosphere. After deaerating for 15 minutes with N_2 gas $Pd_2(dba)_3$ (0.07 equiv.) and BINAP (0.2 equiv.) was added into the solution. Then it was refluxed at 110 °C for 48 hours. After that, the reaction mixture was cooled and the solvent was removed under vacuum. The concentrated reaction mixture was then diluted with distilled water and extracted with dichloromethane (DCM). The combined DCM extracts were washed with brine solution and dried over anhydrous sodium sulfate. After concentrating, it was purified by column chromatography (Silica Gel 100-200 mesh, ethyl acetate/hexane (1:99)) to give the product as dark green solid.

1,4,7,10-tetrakis(3,4,5-tris(decyloxy)phenyl)-1,4,7,10-tetrahydrobenzo[lmn][4,7]phenanthrolino[2,1,10,9-defgh][2,9]phenanthroline-2,3,8,9-tetraone (1):

1,4,5,8-tetrakis((3,4,5-tris(decyloxy)phenyl)amino)anthracene-9,10-dione (**4**) (200 mg, 0.082 mmol, 1 equiv.), diethyl malonate (261.73 mg, 1.63 mmol, 20 equiv.), potassium acetate (64.15 mg, 0.65 mmol, 8 equiv.) and dimethylformamide (DMF) (2 mL) were added in a 10 ml microwave reaction tube under inert atmosphere. The reaction was heated by microwave irradiation to 172 °C for 120 min. Then the crude product was diluted with distilled water and extracted with diethyl ether. The combined DCM extracts were washed with brine solution and dried over anhydrous sodium sulfate. After concentrating, it was purified by column chromatography (Silica Gel 100-200 mesh, ethyl acetate/hexane 8:92)) to give the product. The final product was then dissolved in minimum amount of DCM and precipitated by adding cold methanol. After that, the pure product was obtained as red powder in a yield of 75%.

^{1}H NMR (400 MHz, $CDCl_3$, δ ppm): 7.15 (s, 4H), 6.48 (s, 8H), 4.04 (t, J = 6.56 Hz, 8H), 3.88 (t, J = 6.44/6.52 Hz, 16H), 1.81-1.75 (m, 24H), 1.54-1.38 (m, 48H), 1.28-1.25 (m, 120H), 0.90-0.85 (m, 36H).

^{13}C NMR (100 MHz, $CDCl_3$, δ ppm): 158.69, 154.60, 138.59, 138.21, 137.95, 131.91, 121.61, 114.15, 109.85, 106.55, 73.63, 69.13, 31.97, 31.91, 30.47, 29.79, 29.72, 29.65, 29.62, 29.57, 29.43, 29.35, 29.27, 26.15, 26.10, 22.77, 22.69, 14.14, 14.12.

IR (Neat, KBr, ν_{max}/cm^{-1}): 2924.41, 2854.88, 1703.21, 1592.50, 1563.70, 1498.00, 1465.35, 1437.40, 1373.80, 1311.70, 1223.45, 1115.52, 771.78.

MALDI-MS (m/z): M^+ 2547.5205 (calcd for $C_{164}H_{264}N_4O_{16}$ = 2547.0046).

1,4,7,10-tetrakis(3,4,5-tris(dodecyloxy)phenyl)-1,4,7,10-tetrahydrobenzo[lmn][4,7]phenanthrolino[2,1,10,9-defgh][2,9]phenanthroline-2,3,8,9-tetraone (2):

Compound was synthesized according to a similar procedure to **1.** It was purified by column chromatography (Silica Gel 100-200 mesh, ethyl acetate/hexane (8:92)) to give the product as red powder in 71 % yield.

^{1}H NMR (400 MHz, $CDCl_3$, δ ppm): 7.15 (s, 4H), 6.48 (s, 8H), 4.04 (t, J = 6.48/6.44 Hz, 8H), 3.88 (t, J = 6.52/6.48 Hz, 16H), 1.81-1.75 (m, 24H), 1.52-1.38 (m, 48H), 1.27-1.24 (m, 168H), 0.90-0.85 (m, 36H).

^{13}C NMR (100 MHz, $CDCl_3$, δ ppm): 158.70, 154.60, 138.57, 138.21, 137.95, 131.90, 121.61, 114.15, 109.85, 106.51, 73.62, 69.11, 37.11, 31.97, 31.94, 30.48, 30.43, 30.37, 30.06, 29.80, 29.79, 29.72, 29.71, 29.67, 29.64, 29.43, 29.38, 29.27, 29.20, 29.19, 19.14, 27.11, 26.16, 26.11, 22.73, 22.70, 14.13.

IR (Neat, KBr, ν_{max}/cm^{-1}): 2924.25, 2854.48, 1703.79, 1593.70, 1564.80, 1498.30, 1465.82, 1438.30, 1368.60, 1310.00, 1224.40, 1115.93, 771.80.

MALDI-MS (m/z): M^+ 2883.3562 (calcd for $C_{188}H_{312}N_4O_{16}$ = 2883.3802).

1,4,7,10-tetrakis(3,4,5-tris(tetradecyloxy)phenyl)-1,4,7,10-tetrahydrobenzo[lmn][4,7]phenanthrolino[2,1,10,9-defgh][2,9]phenanthroline-2,3,8,9-tetraone (3):

Compound was synthesized according to a similar procedure to **1.** It was purified by column chromatography (Silica Gel 100-200 mesh, ethyl acetate/hexane (8:92)) to give the product as red powder solid in 73 % yield.

^{1}H NMR (400 MHz, $CDCl_3$, δ ppm): 7.15 (s, 4H), 6.48 (s, 4H), 4.04 (t, J = 6.56 Hz, 8H), 3.87 (t, J = 6.4/6.44 Hz, 16H), 1.81-1.75 (m, 24H), 1.53-1.38 (m, 48H), 1.26-1.24 (m, 216H), 0.90-0.85 (m, 36H).

^{13}C NMR (100 MHz, $CDCl_3$, δ ppm): 158.70, 154.61, 138.58, 138.21, 137.95, 131.90, 121.61, 114.15, 109.85, 106.52, 73.62, 69.12, 31.96, 31.95, 30.48, 29.81, 29.79, 29.69, 29.65, 29.55, 29.42, 29.39, 29.28, 26.16, 26.12, 22.72, 22.71, 14.13.

IR (Neat, KBr, ν_{max}/cm^{-1}): 2923.47, 2853.70, 1702.20, 1595.30, 1498.20, 1465.10, 1436.50, 1381.60, 1313.80, 1222.00, 1115.90, 771.73.

MALDI-MS (m/z): M^+ 3219.9165 (calcd for $C_{212}H_{360}N_4O_{16}$ = 3219.7558).

2) NMR Spectra:

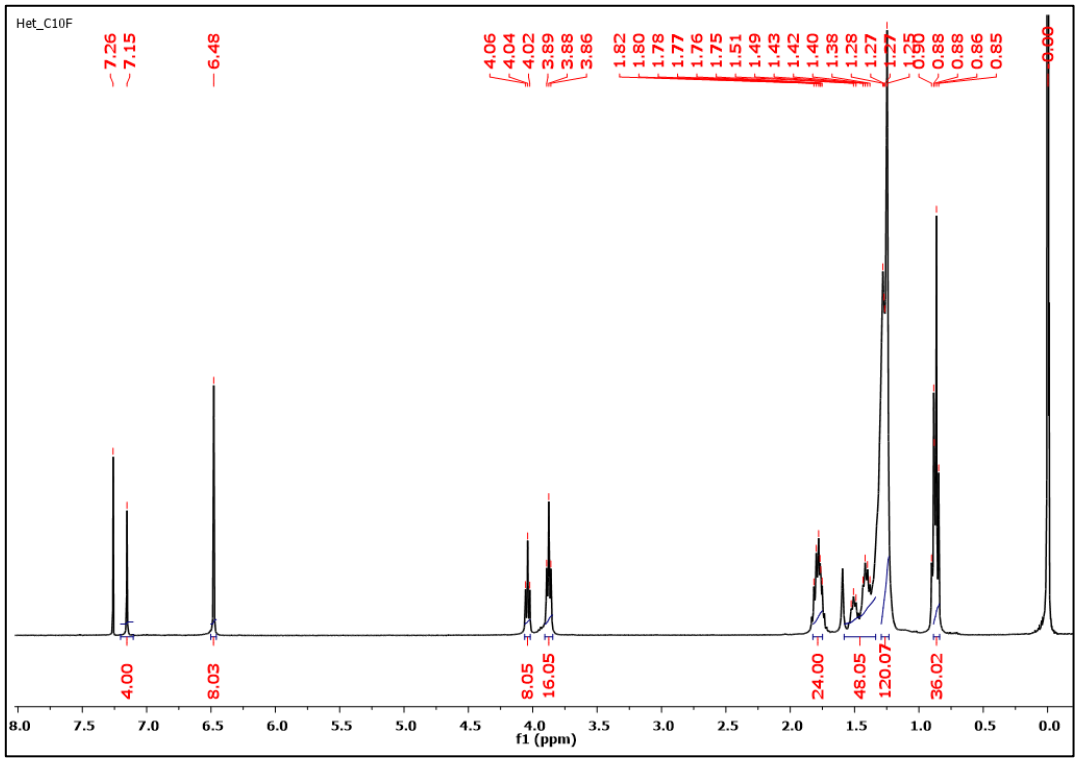

Figure S1. ^{1}H NMR of 1,4,7,10-tetrakis(3,4,5-tris(decyloxy)phenyl)-1,4,7,10-tetrahydrobenzo[lmn][4,7]phenanthrolino[2,1,10,9-defgh][2,9]phenanthroline-2,3,8,9-tetraone (**1**).

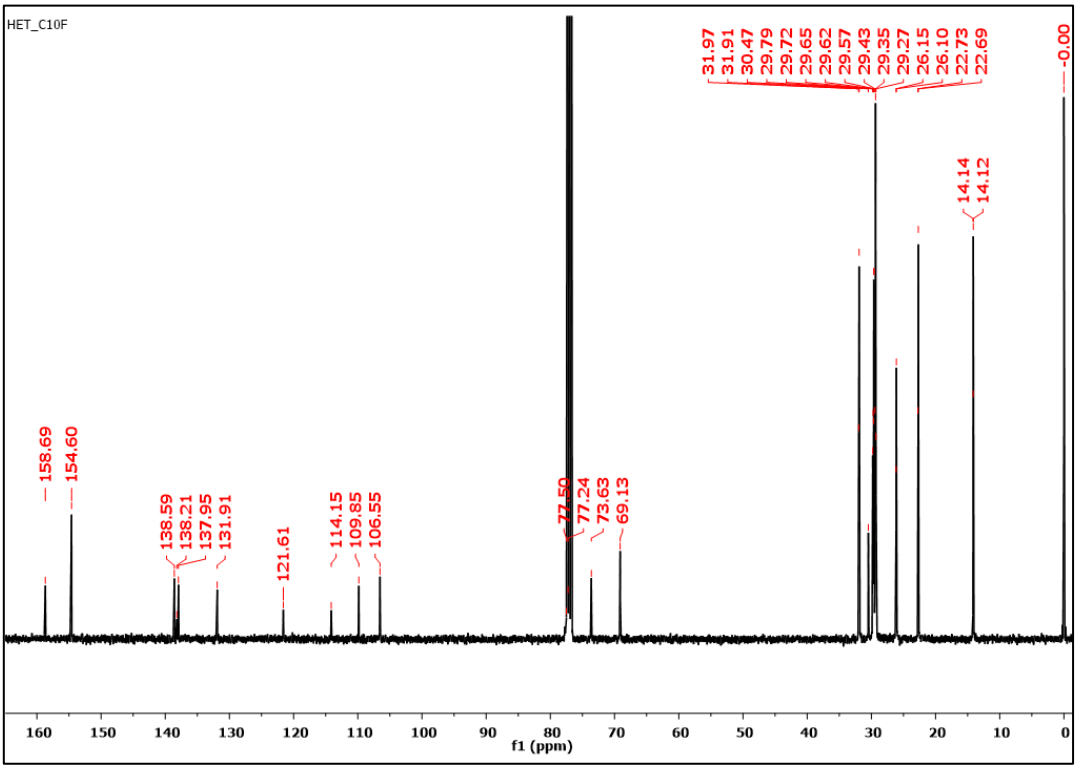

Figure S2. ^{13}C NMR of 1,4,7,10-tetrakis(3,4,5-tris(decyloxy)phenyl)-1,4,7,10-tetrahydrobenzo[lmn][4,7]phenanthrolino[2,1,10,9-defgh][2,9]phenanthroline-2,3,8,9-tetraone (**1**).

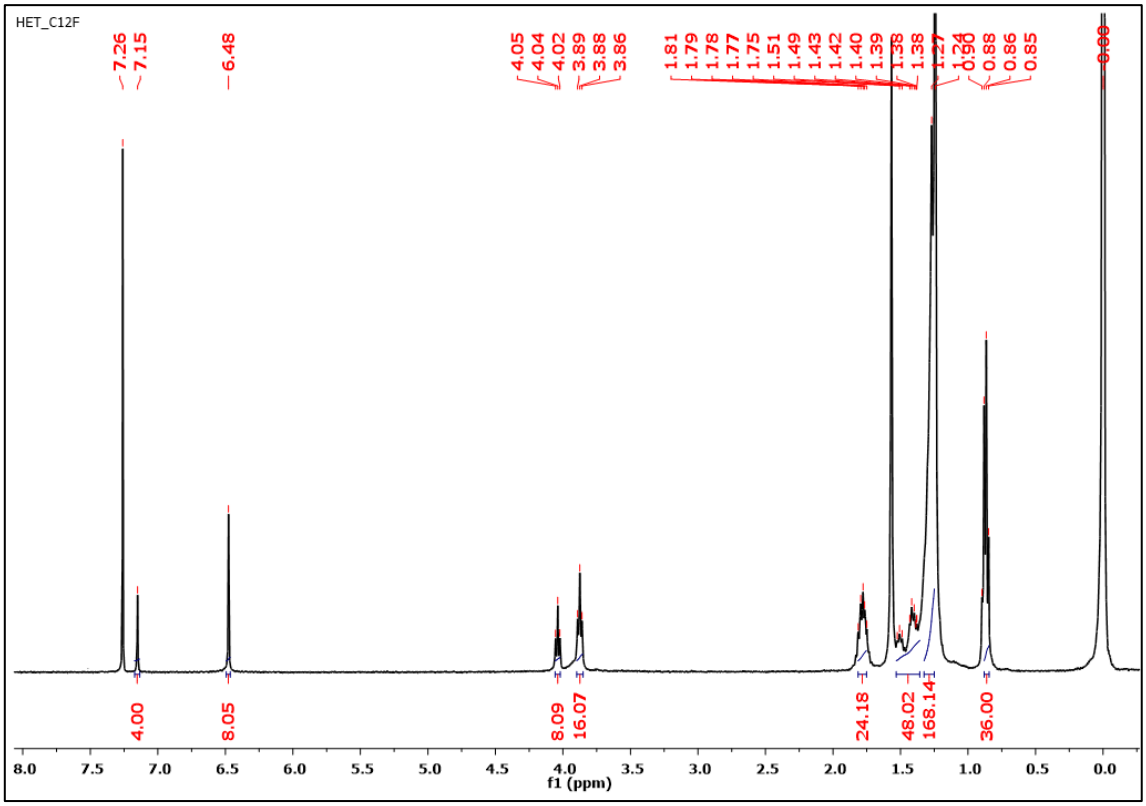

Figure S3. ^{1}H NMR of 1,4,7,10-tetrakis(3,4,5-tris(dodecyloxy)phenyl)-1,4,7,10-tetrahydrobenzo[lmn][4,7]phenanthrolino[2,1,10,9-defgh][2,9]phenanthroline-2,3,8,9-tetraone (**2**).

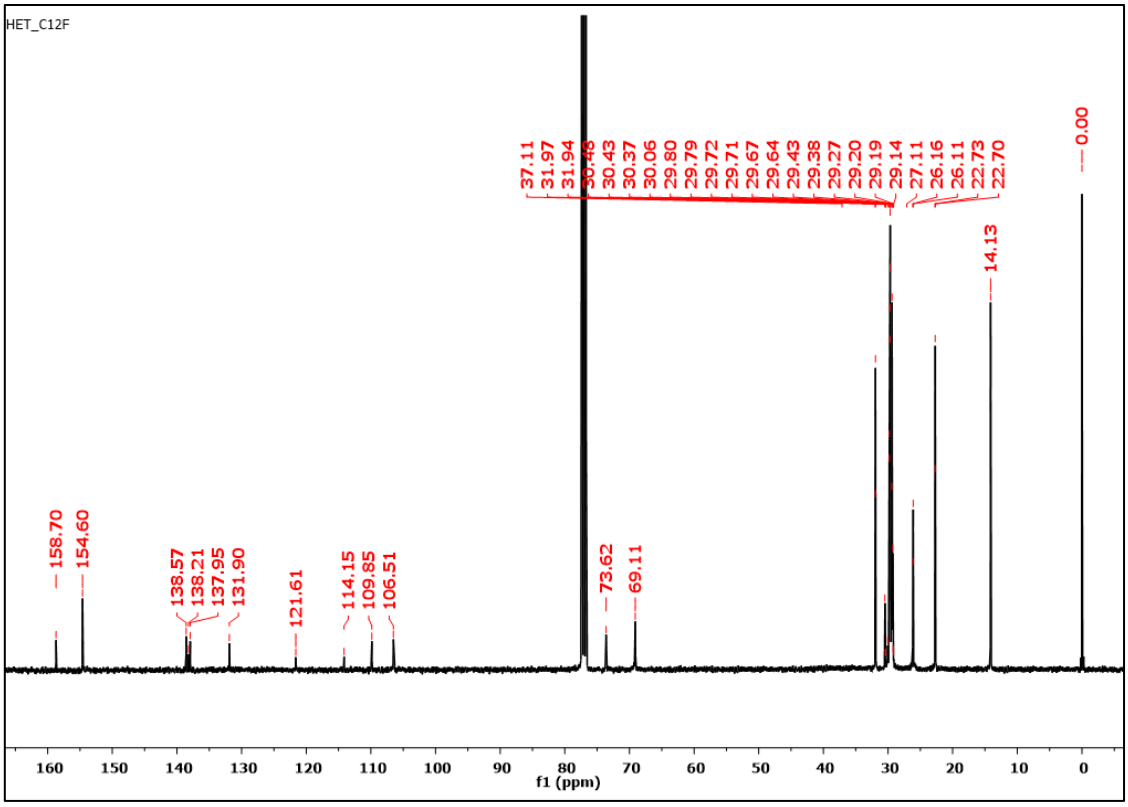

Figure S4. ^{13}C NMR of 1,4,7,10-tetrakis(3,4,5-tris(dodecyloxy)phenyl)-1,4,7,10-tetrahydrobenzo[lmn][4,7]phenanthrolino[2,1,10,9-defgh][2,9]phenanthroline-2,3,8,9-tetraone (**2**).

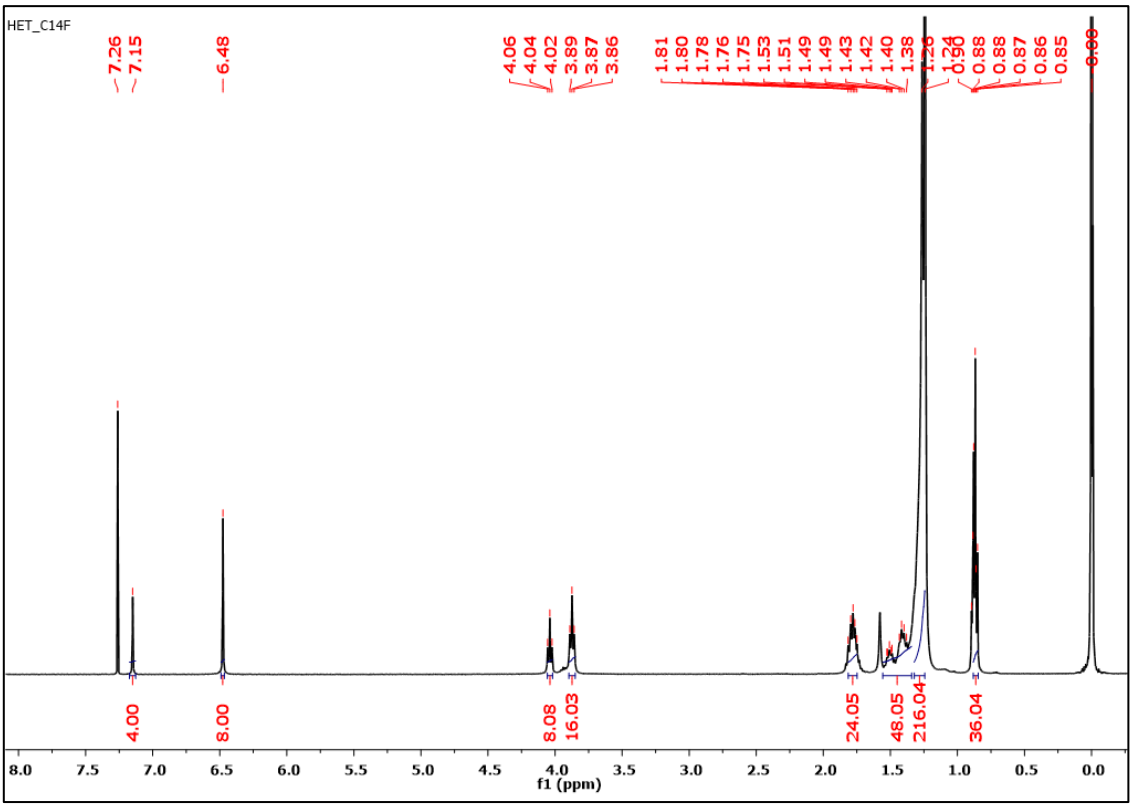

Figure S5. ^{1}H NMR of 1,4,7,10-tetrakis(3,4,5-tris(tetradecyloxy)phenyl)-1,4,7,10-tetrahydrobenzo[lmn][4,7]phenanthrolino[2,1,10,9-defgh][2,9]phenanthroline-2,3,8,9-tetraone (**3**).

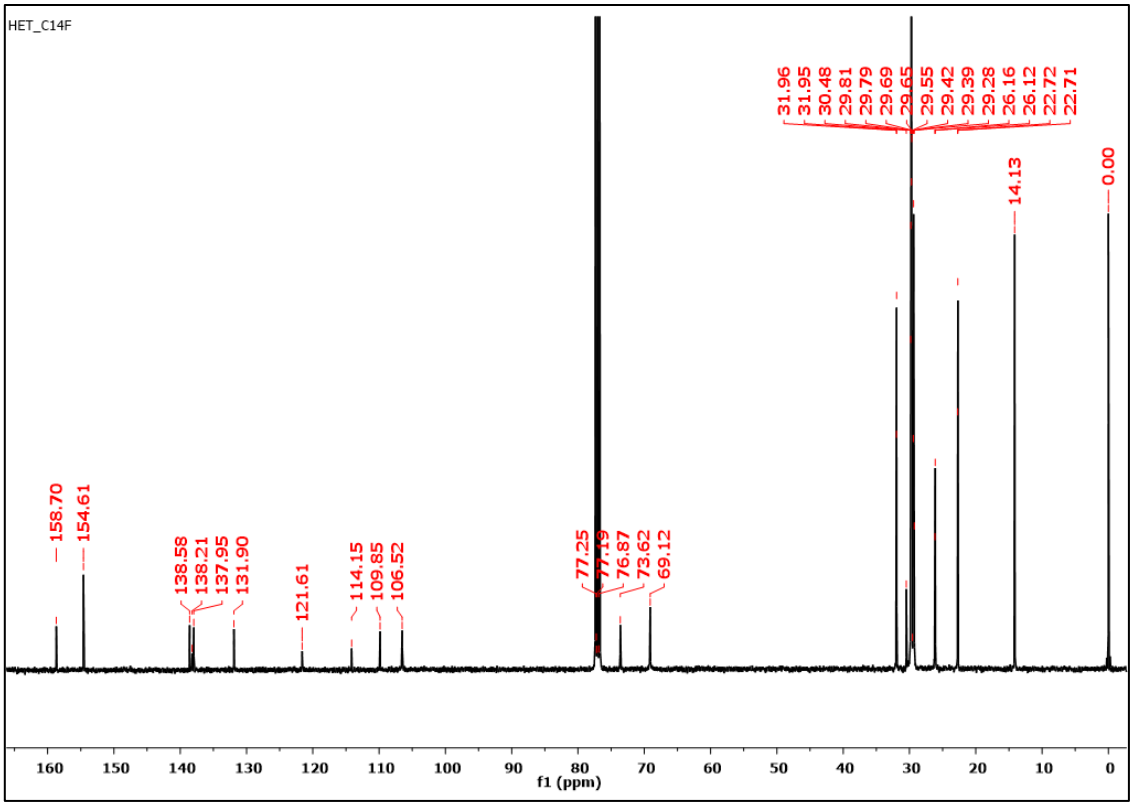

Figure S6. ^{13}C NMR of 1,4,7,10-tetrakis(3,4,5-tris(tetradecyloxy)phenyl)-1,4,7,10-tetrahydrobenzo[lmn][4,7]phenanthrolino[2,1,10,9-defgh][2,9]phenanthroline-2,3,8,9-tetraone (**3**).

3) TGA Curves:

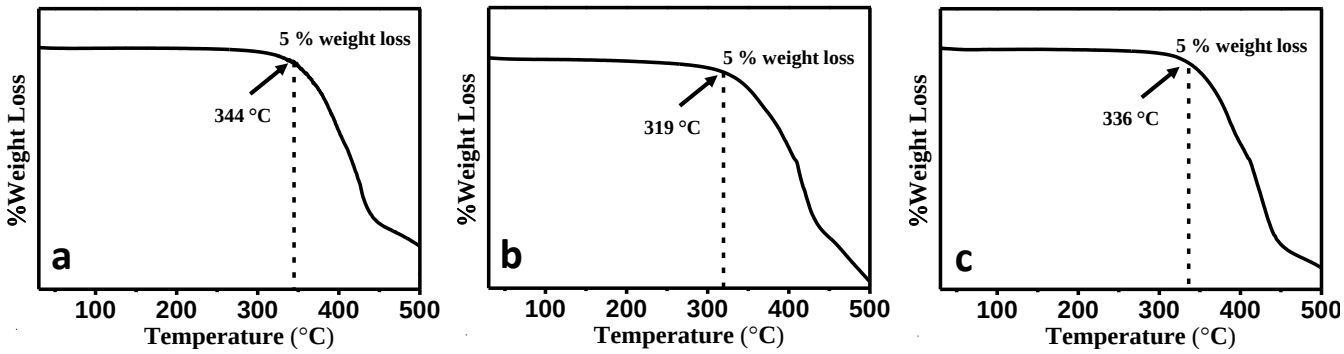

Figure S7. TGA curves of (a) **1**, (b) **2** and (c) **3**. The measurements were performed under a nitrogen atmosphere, with heating and cooling rates of 10 °C/min.

4) DSC Thermograms:

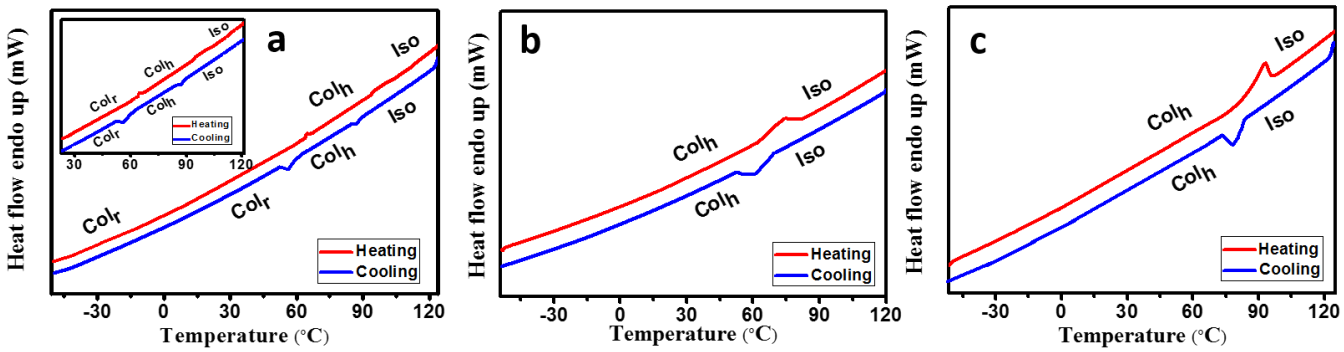

Figure S8. DSC thermogram of compounds (a) **1**, (b) **2** and (c) **3.** The measurements were performed under a nitrogen atmosphere, with heating and cooling rates of 10 °C/min.

Table S1. Experimental data of thermal properties of compounds **1 - 3.**[a,b]

Mesogen	Heating Scan	Cooling Scan
1	Col_r 64.7 (1.92) Col_h 94.9 (6.50) I	I 88.6 (3.26) Col_h 55.8 (1.46) Col_r
2	Col_h 73.7 (23.51) I	I 60.3 (17.19) Col_h
3	Col_h 93.1 (91.87) I	I 78.1 (60.30) Col_h

[a] Transition temperatures (peak, in °C) and associated enthalpy changes in brackets in kJ mol^{-1}. [b] Transition temperatures from DSC. Abbreviations: Col_r = Columnar rectangular, Col_h = Columnar hexagonal, I = isotropic liquid.

5) POM Studies:

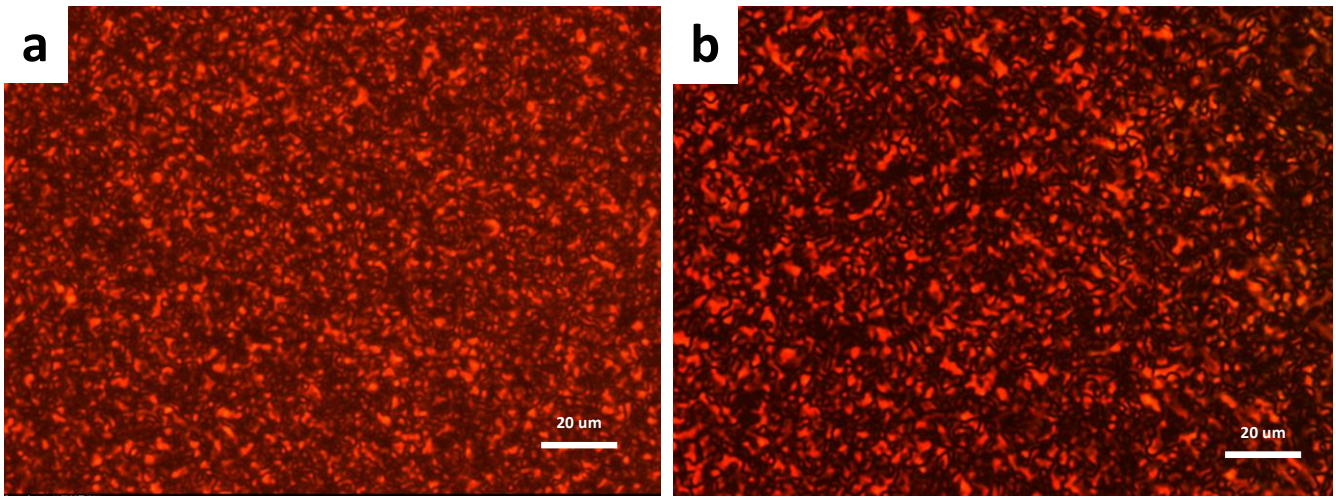

Figure S9. Polarising optical micrographs of compound (a) **2** at 26.7 °C and (b) **3** at 27.2 °C, on cooling from isotropic liquid kept between a glass slide and coverslip (crossed polarizers, magnification X 500).

6) X-ray diffraction studies:

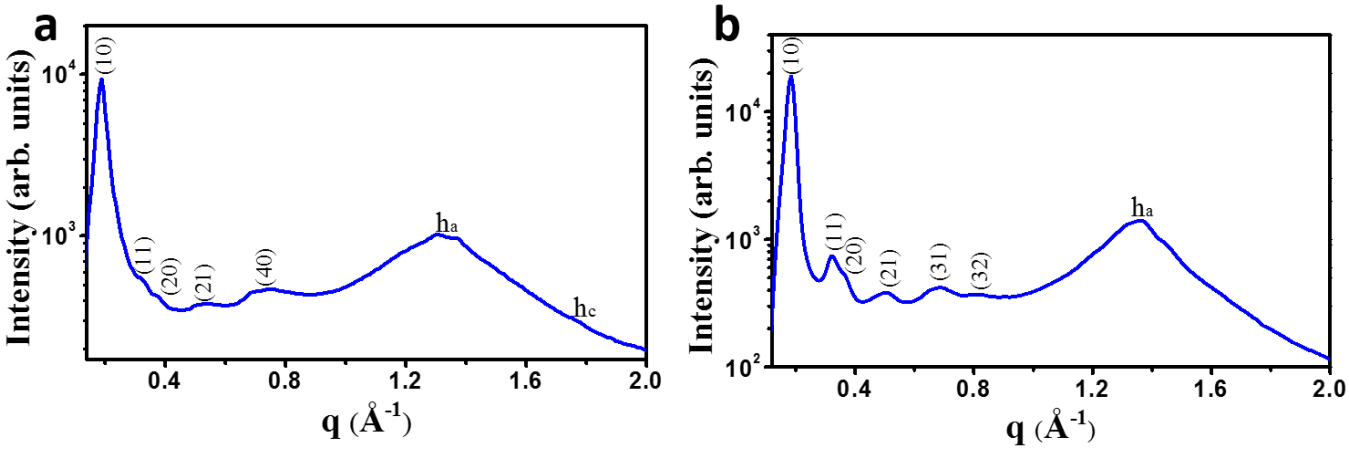

Figure S10. X-ray diffraction pattern of compound (a) **2** at 25 °C and (b) **3** at 25 °C on cooling from the isotropic liquid.

Correlation length: The correlation length, the degree of order within the mesophases, was calculated using $\xi = [k\ 2\pi]/[(\Delta q)]$ which is equivalent to Scherrer's equation, $\xi = [k\ \lambda]/[(\Delta 2\theta)\ \mathrm{Cos}\theta]$. Here, k is the shape factor whose typical value is 0.89, λ is the wavelength of the incident X-ray, $\Delta 2\theta$ is the broadening in 2θ at half of the maximum intensity (FWHM) with radian unit, and θ is the maximum of the reflection. q is the scattering vector ($q = 4\pi \mathrm{Sin}\theta/\lambda$) and Δq is the broadening in q at half of the maximum intensity. Δq is obtained by Lorentzian fitting of the diffraction pattern.[1]

Electron density map: The electron density ρ(x,y) of a liquid crystal is linked to its structure factor F(hk) by inverse Fourier transformation:

$$\rho(x,y) = \sum_{h\,k} F(hk)\, e^{2\pi i(hx+ky)}$$

In this formula (hk) are the Miller Indices and x, y are the fractional coordinates in the unit cell. To calculate the electron density, the complex structure factor (hk) has to be written as the product of the phase Φ(hk) and the modulus |(hk)| which is proportional to the square root of the intensity I(hk) of the observed reflection

$$F(hk) = |F(hk)|e^{i\Phi(hk)} = \sqrt{I(hk)}e^{i\Phi(hk)}$$

While the intensity I(hk) can be easily obtained from the X-ray diffraction experiment, the only information that cannot be obtained directly from the experiment is the phase Φ(hk) for each diffraction peak. However, this problem becomes easily tractable when the structure under study is centro-symmetric, that if *ρ(x,y)=ρ(-x,-y)*, *F*(hk) can only be real hence, $\phi(hk)$ can only be 0 or π. For non centro-symmetric groups, the phase may take every value between 0 and 2π. The observed columnar phases in the present case in compound **1**-**3** are centro-symmetric and also having few reflections in the small angle region. Therefore, it is easy to reconstruct electron density maps of all possible phase combinations. The "correct" map is subsequently chosen on the merit of the reconstructed maps and other physical and chemical knowledge of the system such as chemical constituents and their sizes *etc*.[1]

Table S2: The Indices, observed and calculated *d*-spacings and planes of the diffraction peaks of the centered rectangular lattice observed at 25 °C for compound **1**. The lattice parameters are a = 58.72 Å, b = 41.26 Å. h_a is due to chain-chain correlation. h_c due to core to core (face to face) correlations. d_{obs}: experimental *d*-spacing; d_{cal}: calculated *d*-spacing by using the relation:$\frac{1}{d^2} = (\frac{h^2}{a^2} + \frac{k^2}{b^2})$ with $h+k = 2n$, n ε Z, Z is an integer; h, k are the Miller indices.

(hk)	***d-spacing Experimental d_{obs} (Å)***	***d-spacing Calculated d_{cal} (Å)***	***Intensity***	***Phase (Φ)***	***Multiplicity***
20	29.36	29.36	100.00	0	2
02	20.63	20.63	11.04	0	2
22	16.84	16.88	2.53	π	4
40	14.65	14.68	2.15	π	2
13	13.13	13.39	1.81	π	4
04	10.37	10.31	2.04	0	2
35	7.98	7.60	2.44	π	4
h_a	4.84				
h_c	3.60				

Table S3: The Indices, observed and calculated *d*-spacings and planes of the diffraction peaks of the hexagonal lattice observed at 70 °C for compound **1**. The lattice parameter is a = 32.02 Å. h_a is due to

chain-chain correlation. h_c due to core to core (face to face) correlations. d_{obs}: experimental *d*-spacing; d_{cal}: calculated *d*-spacing by using the relation:$\frac{1}{d^2} = \frac{4}{3}(\frac{h^2+hk+k^2}{a^2})$; *h*, *k* are the Miller indices.

(hk)	***d-spacing Experimental d_{obs} (Å)***	***d-spacing Calculated d_{cal} (Å)***	***Intensity***	***Phase (Φ)***	***Multiplicity***
10	27.73	27.73	100.00	0	6
11	16.12	16.01	2.81	0	6
20	13.89	13.86	1.81	π	6
21	10.63	10.48	1.85	π	12
22	8.17	8.00			
h_a	4.84	--			

Table S4: The Indices, observed and calculated *d*-spacings and planes of the diffraction peaks of the hexagonal lattice observed at 25 °C for compound **2**. The lattice parameter is a = 38.64 Å. h_a is due to chain-chain correlation. h_c due to core to core (face to face) correlations. d_{obs}: experimental *d*-spacing; d_{cal}: calculated *d*-spacing by using the relation:$\frac{1}{d^2} = \frac{4}{3}(\frac{h^2+hk+k^2}{a^2})$; *h*, *k* are the Miller indices.

(hk)	***d-spacing Experimental d_{obs} (Å)***	***d-spacing Calculated d_{cal} (Å)***	***Intensity***	***Phase (Φ)***	***Multiplicity***
10	33.47	33.46	100.00	0	6
11	19.34	19.32	5.75	0	6
20	16.55	16.73	4.55	π	6
21	12.41	12.65	4.03	0	12
40	8.64	8.37	4.97	π	6
h_a	4.84	--			
h_c	3.53	--			

Table S5: The Indices, observed and calculated *d*-spacings and planes of the diffraction peaks of the hexagonal lattice observed at 25 °C for compound **3**. The lattice parameter is a = 39.01 Å. h_a is due to chain-chain correlation. d_{obs}: experimental *d*-spacing; d_{cal}: calculated *d*-spacing by using the relation:$\frac{1}{d^2} = \frac{4}{3}(\frac{h^2+hk+k^2}{a^2})$; *h*, *k* are the Miller indices.

(hk)	***d-spacing Experimental d_{obs} (Å)***	***d-spacing Calculated d_{cal} (Å)***	***Intensity***	***Phase (Φ)***	***Multiplicity***
10	33.78	33.78	100.00	0	6
11	19.53	19.51	3.88	0	6
20	17.07	16.89	2.77	π	6
21	12.56	12.77	2.01	0	12
31	9.24	9.37	2.21	π	12
32	7.66	7.75			
h_a	4.59	--			

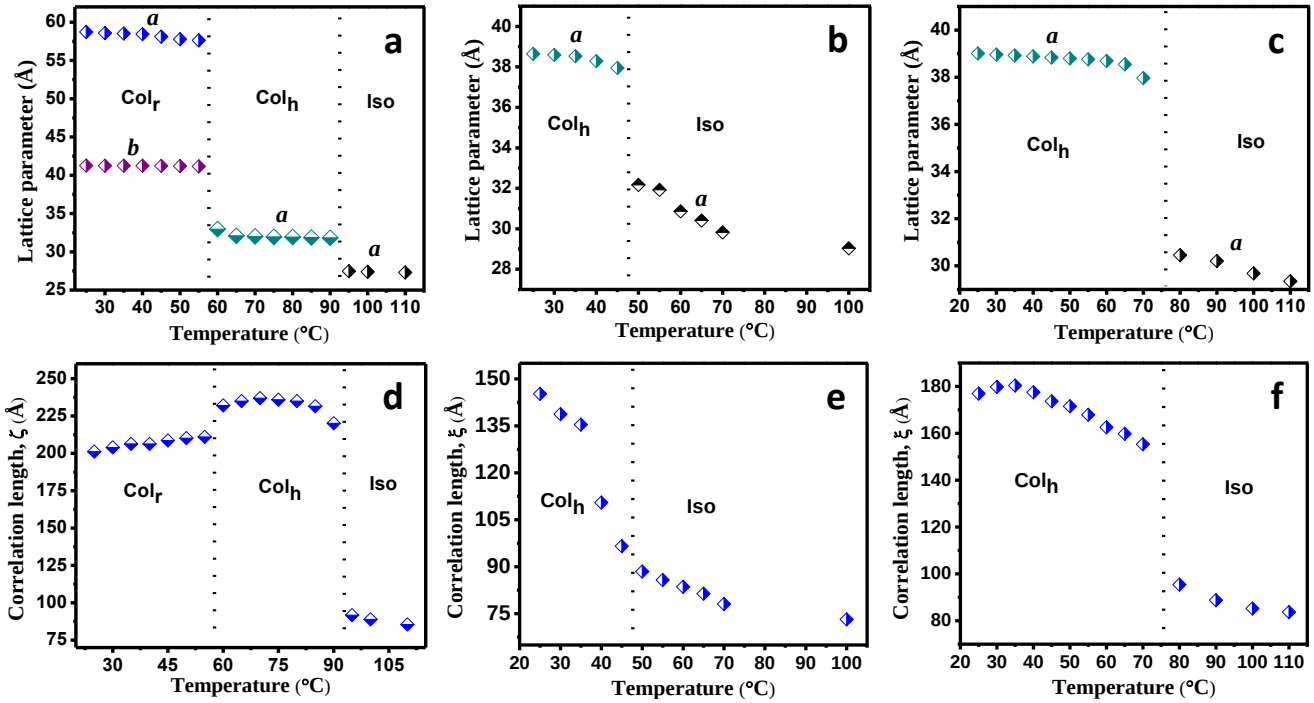

Figure S11. Variation of lattice parameter of compound (a) **1**, (b) **2** and (c) **3** with temperature. In the Col_r phase, *a* and *b* represents the basis of the lattice and in the Col_h phase *a* shows the inter-columnar separation and in the Iso (Isotropic) phase *a* is the average molecular separation. Variation of correlation length of compound (d) **1**, (e) **2** and (f) **3** with temperature. The correlation length is calculated by using (20) (Col_r), (10) (Col_h) and first peak of the small angle for isotropic (Iso) phase.

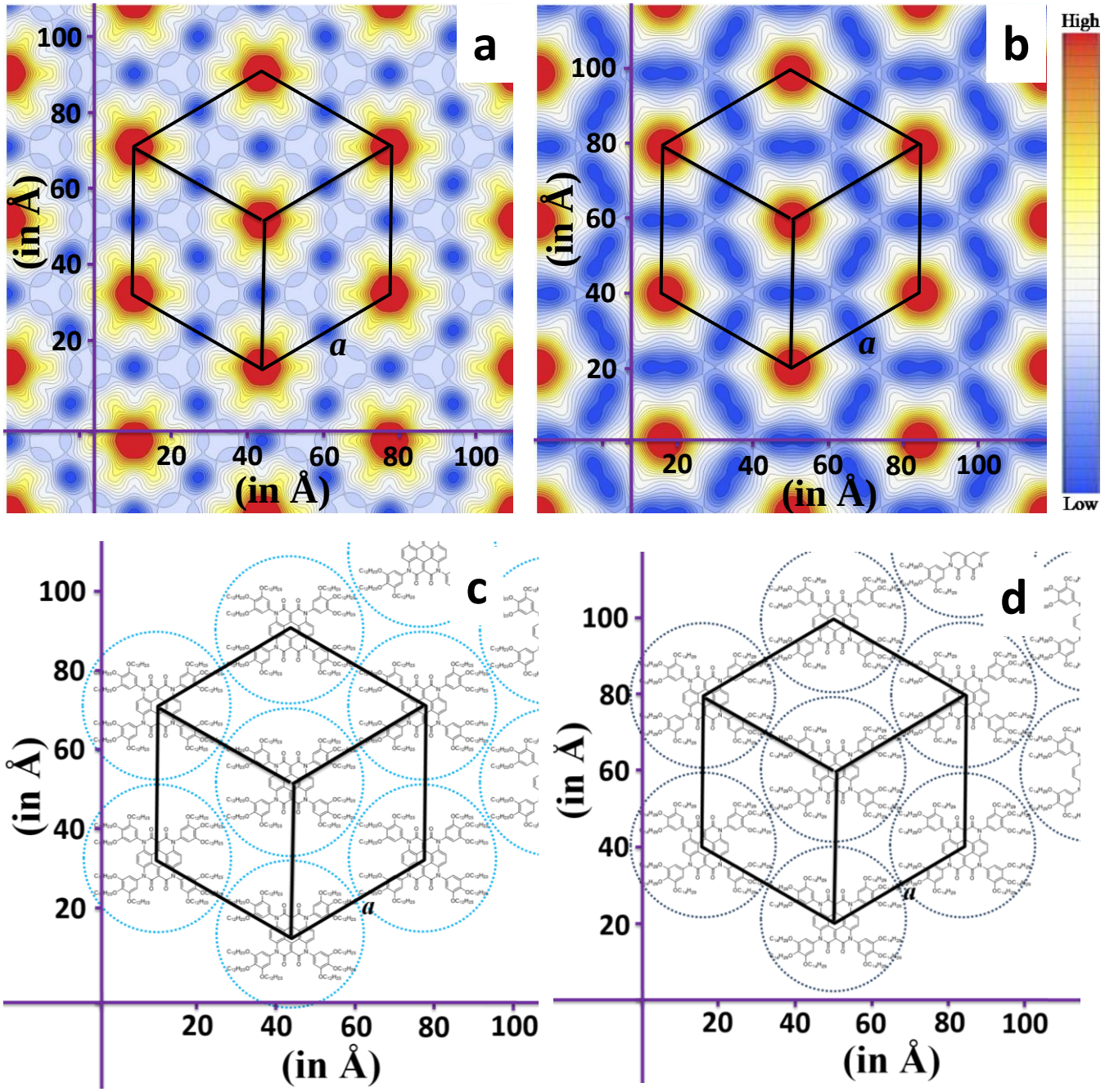

Figure S12. Electron density map of Col_h mesophase of compound (a) **2** and (b) **3** at temperature 25 ºC. And the corresponding arrangement of the molecules in the lattice is shown in (c) & (d), respectively.

7) Photophysical studies:

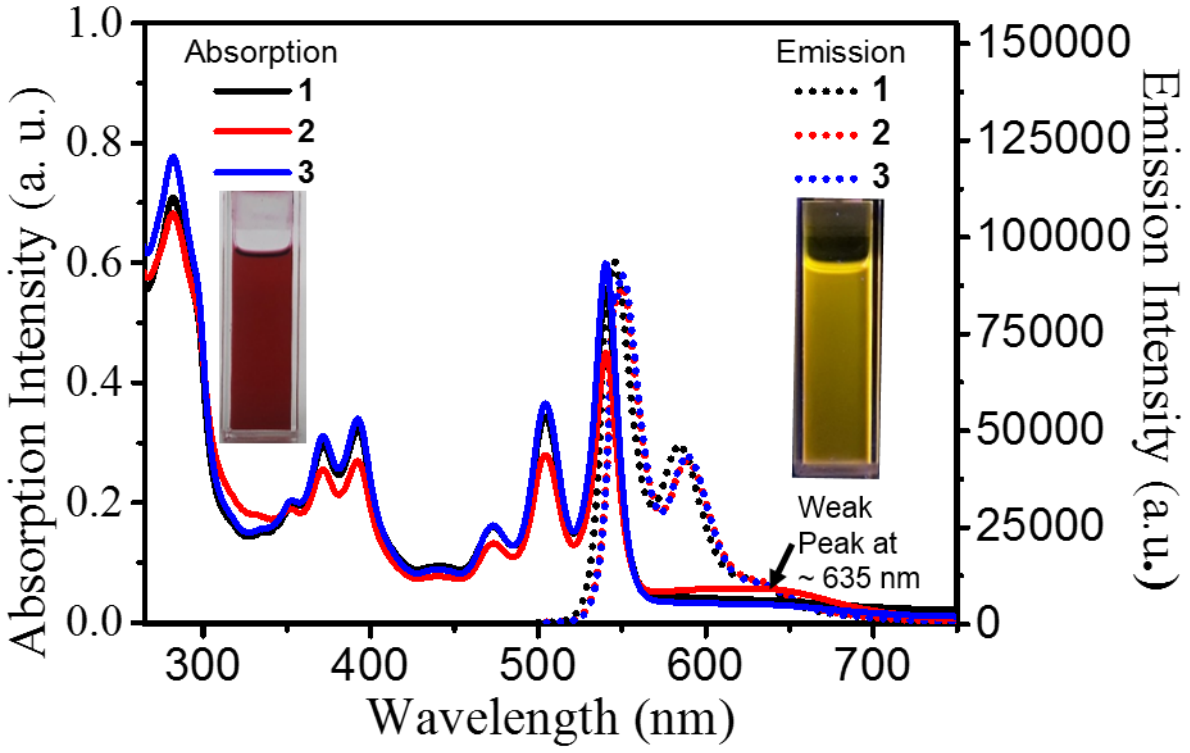

Figure S13. Absorption and emission spectra of **1-3** in solution state (Inset show the corresponding red colour emission in daylight and yellow colour in 365 nm UV light).

Table S6: Experimental data of photophysical properties of compounds **1-3.**[a]

Mesogens	Absorption (nm)	Emission[b] (nm)
1	282, 352, 371, 392, 473, 504, 540, 635	546, 550, 589, 635
2	282, 352, 371, 392,473, 504, 540, 634	546, 550, 589, 635
3	282, 352, 372, 392, 473, 504, 540, 637	541, 548, 585, 628

[a] Measured in $CHCl_3$ solution at concentrations of approximately 10^{-6} M. [b] Corresponding to excitation wavelength 540 nm.

8) Electrochemical studies:

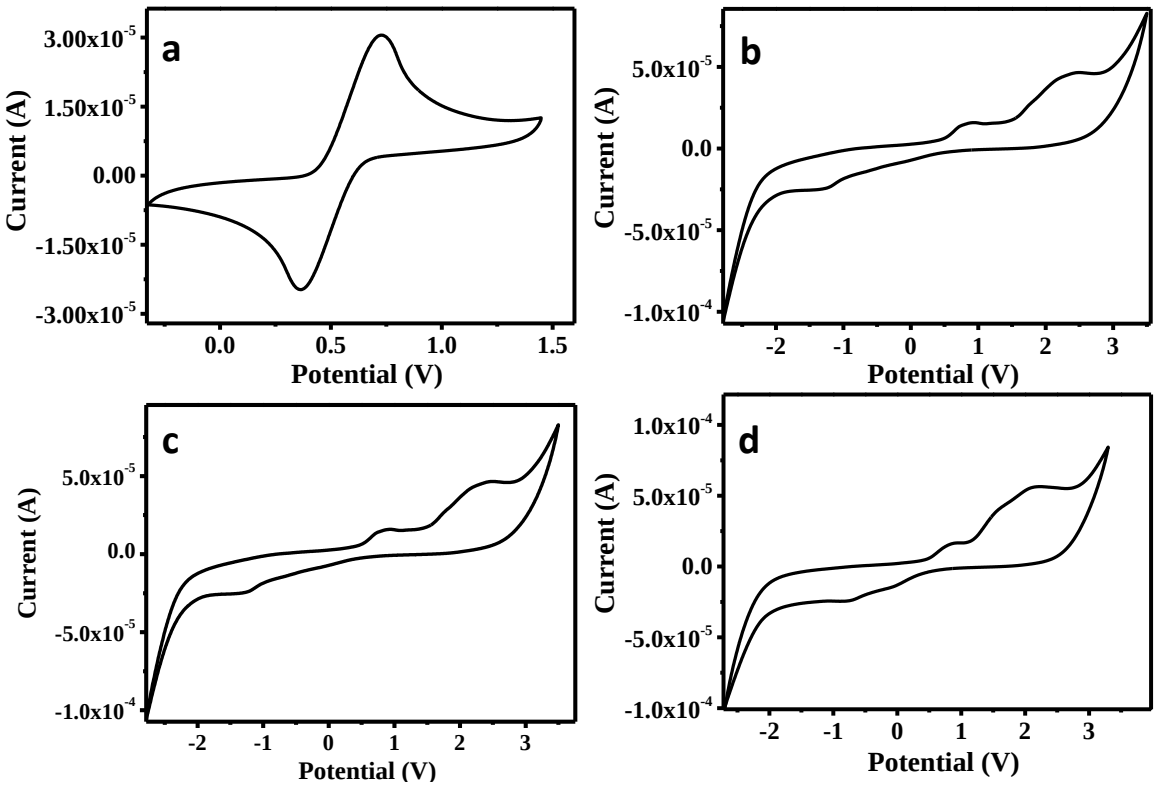

Figure S14. Cyclic Voltammograms of (a) ferrocene, compounds (b) **1**, (c) **2**, and (d) **3** in HPLC DCM solution of tetrabutylammonium hexafluorophosphate (0.1 M) at a scanning rate 50 mVs^{-1}.

Table S7. Electrochemical properties of compounds **1-3**[a].

Mesogen	$\lambda_{onset\ (UV,\ nm)}$	$\Delta E_{g,\ UV}$[b,c]	$E_{ox,onset}$[b]	$E_{red,onset}$[b]	E_{HOMO}[b,d]	E_{LUMO}[b,e]	$\Delta E_{g,CV}$[b,f]	$\Delta E_{g,DFT}$[b,g]
1	755	1.64	0.59	-0.80	-4.90	-3.51	1.39	2.32
2	746	1.66	0.58	-0.80	-4.89	-3.51	1.38	2.35
3	766	1.62	0.57	-0.54	-4.88	-3.77	1.11	2.31

[a] Experimental conditions: $Ag/AgNO_3$ as reference electrode, platinum wire as counter electrode, glassy carbon as working electrode, tetrabutylammonium perchlorate (0.1 M) as supporting electrolyte, room temperature. [b] Electron volts (eV). [c] Band gap determined from the red edge of the longest wavelength in the UV-visible absorption spectra. [d] Estimated from the formula $E_{HOMO} = -(4.8 - E_{1/2,Fc,Fc^+} + E_{oxd,onset})$ eV. [e] Estimated from the onset reduction peak values using $E_{LUMO} = -(4.8 - E_{1/2,Fc,Fc^+} + E_{red,onset})$ eV. [f] Estimated from the formula $\Delta E_{g,CV} = E_{LUMO} - E_{HOMO}$. [g] HOMO-LUMO energy gap calculated from DFT studies.

For compounds **1**/**2**/**3**, the two peaks in the oxidation cycle with peak potentials at 0.94/0.93/0.92 V and 2.44/2.46/2.20 V while one peak in reduction wave at -1.26/-1.28/-0.82 V was observed. The energy levels LUMO and HOMO were estimated at -3.51/-3.51/-3.77 eV and -4.90/-4.89/-4.88 eV, based on the reduction and first oxidation onsets, respectively. Both the energy levels are highly favorable for the hole and electron charge carrier injections from the respective suitable electrodes. These results indicating the ambipolar charge transport behavior of the heterocoronene derivatives. The electrochemical energy gaps for compound **1**/**2**/**3** were 1.39/1.38/1.11 eV.

9) Computational studies:

To understand the electronic properties and frontier molecular orbital energy level of compound **1-3** theoretical calculations were carried out with Gaussian 09 suite of packages.[3] A full optimization was carried out using the hybrid functional, Becke's three parameter exchange and the LYP Correlation Functional (B3LYP)[4] at a split valence basis set 6-31G(d,p).

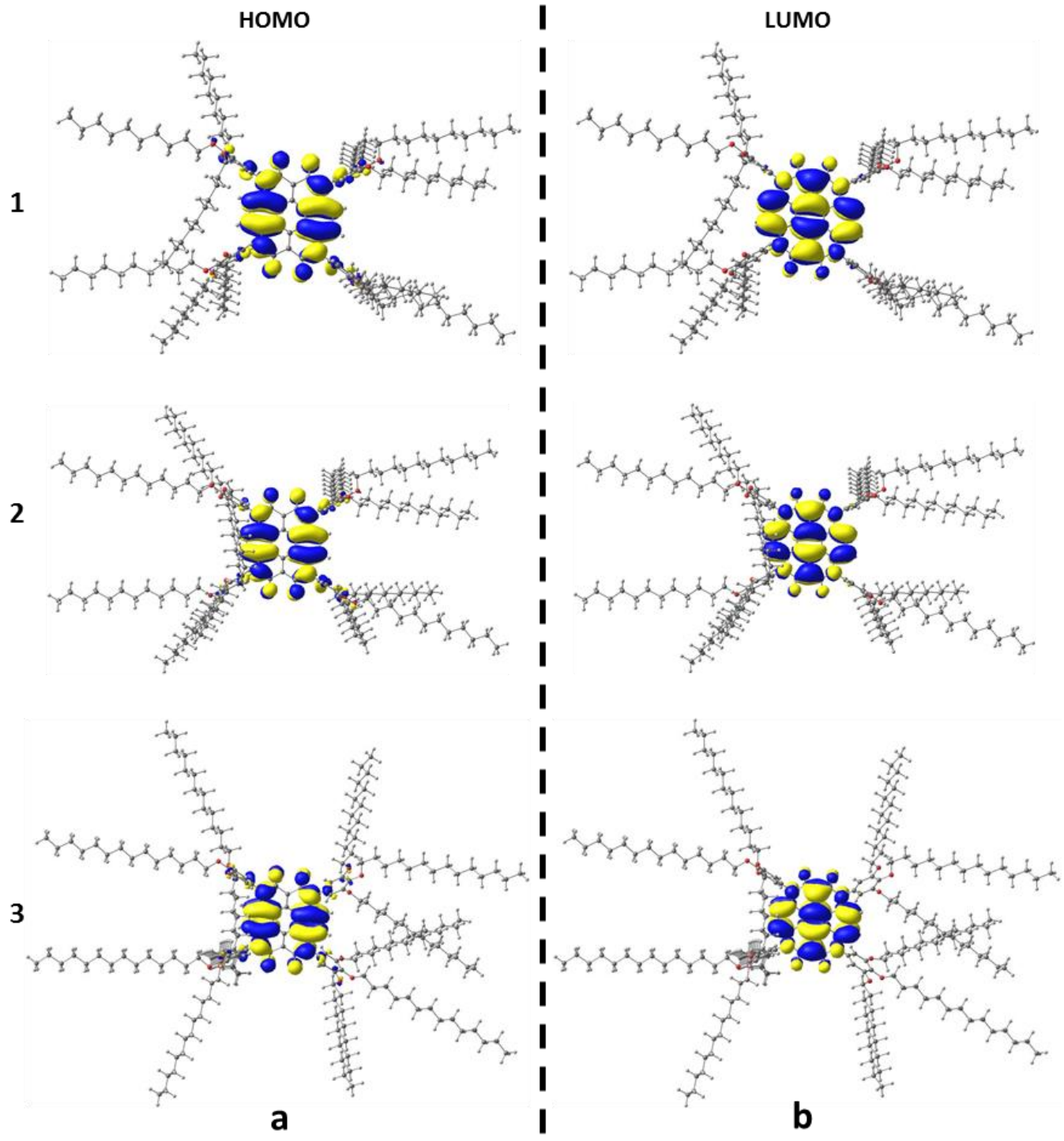

Figure S15. (a) HOMO and (b) LUMO frontier molecular orbitals of compounds **1-3** at the B3LYP/6-31G (d,p) level.

10) SCLC Measurements:

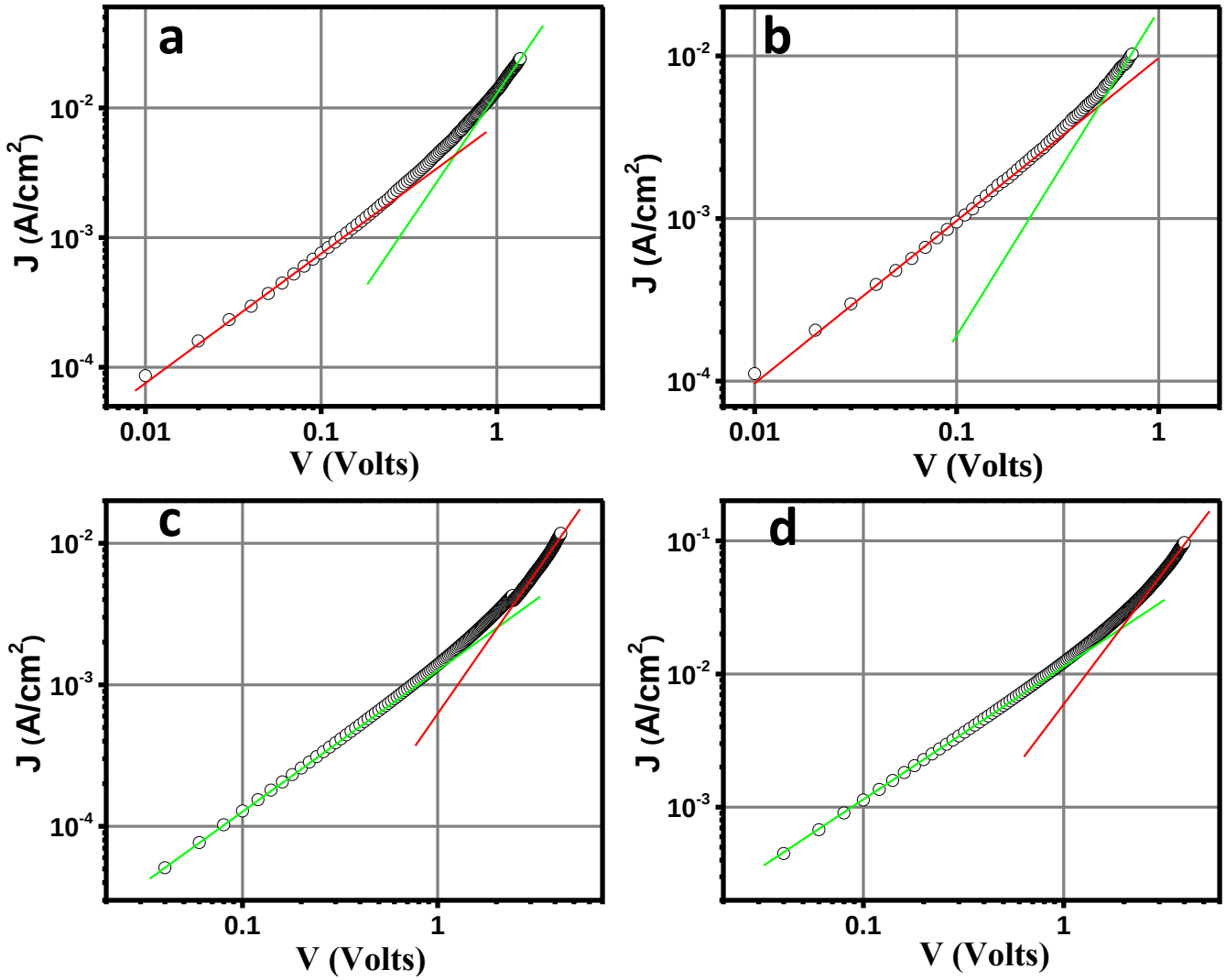

Figure S16. SCLC Current/Voltage characteristics for hole mobility of (a) **2** & (b) **3** and electron mobility of (c) **2** & (d) **3** with fitted two straight lines of slope 1 and 2 depicting Ohmic and SCLC regimes.

Cells for SCLC mobility measurement were prepared using two electrodes on glass substrates, one UV ozone treated patterned ITO and another one as Au electrode. ITO coated glass substrates (10 Ω/cm^2, Xinyan Technologies) were first patterned using zinc powder and 2M HCl solution. Patterned ITO substrates were then cleaned in ultrasonicator using soap solution (5% HelmanexIII soap solution in distilled water), distilled water, acetone and ethanol sequentially for 20 min each. Cleaned ITO substrates were then placed in UV Ozone cleaner at room temperature for 20 minutes before being used for cell fabrication. Au substrates were prepared by sputtering (Tecport sputtering unit) 10 nm of Ni followed by 100 nm of Au layer on a cleaned glass substrates respectively. Cells were assembled using 2 µm thick mylar sheet. The typical thickness of the samples was between 3 to 7.15 µm, measured using interferometry (Perkin Elmer lambda 35). Cells for SCLC measurements were prepared using capillarity.

Empty cells were filled by heating the compound slightly above the melting point on hot plate and were cooled down to room temperature by turning off the hot plate. Current-Voltage measurement and dielectric constant of the samples were measured using Keithley 4200 SCS parametric analyzer. Current-voltage characteristics of all the samples under study showed the standard behavior observed in SCLC cases, showing an Ohmic and quadratic regime at lower and higher voltages respectively. Typical SCLC J-V curve obtained in hole-only and electron-only cells for **2** and **3** is shown in Figure S16.

For hole mobility measurements samples were prepared using patterned Gold and patterned ITO on glass substrates. Gold was chosen as injecting electrode for hole mobility as HOMO ranging 4.90 eV to 4.88 eV for reported compounds closely matches well with that of Gold (~ 5.1eV). Simultaneously, ITO was used as a counter electrode (work function ~ 4.6 eV) with a significant energy gap between LUMO and ITO to ensure a non-injecting electrode for an opposite sign of charges. Cells for electron mobility measurements were prepared exactly as reported by Golemme et al[5] with ZnO coated patterned ITO substrates on both sides to ensure electron only devices. The thickness of all the cells used (for electron and hole) were ranging between 3 to 7.15 µm measured using interferometry technique (*vide infra*). Prepared cells (for hole and electron mobility) were then filled using capillarity by heating the compounds above their respective isotropic transition temperature and then cooling to room temperature.

In SCLC measurement at low applied voltages, the current is a linear function of voltage (current follows the Ohm's law) and the resistive behavior is Ohmic which is given by the following equation.

$$J = ne\mu\frac{V}{d} \qquad \text{(a)}$$

where J is the current density, n is the charge carrier density, e is the elementary charge, μ is the charge carrier drift mobility, V is the applied voltage and d is the thickness of the sample.

At higher voltages, when applied voltage crosses the threshold voltage (V_T), the space charge build up takes place across the sample due to injected charges and the voltage dependence of the current goes to quadratic (slope 2) (Figure S17) which can be approximated by the Mott-Gurney equation given by

$$J = \frac{9}{8}\varepsilon\varepsilon_0\mu\frac{V^2}{d^3} \qquad \text{(b)}$$

where ε_0 is the free space permittivity and ε is the relative dielectric constant of the material. By knowing the thickness (d) and dielectric constant (ε) of the samples we can calculate the mobility.

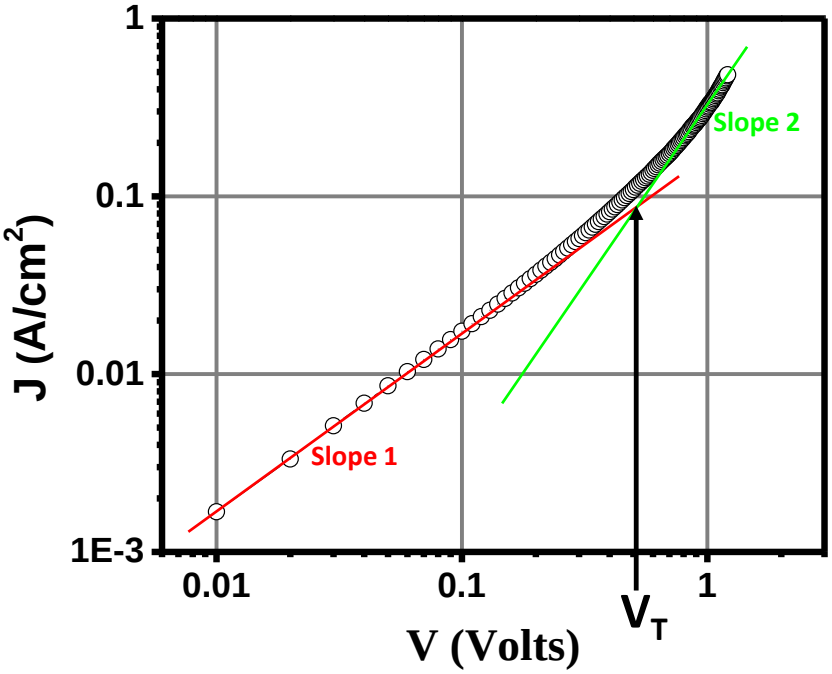

Figure S17: Typical J-V characteristics plot in hole-only cell for compound **1** obtained in SCLC measurement showing Ohmic (Slope 1) and SCLC (Slope 2) regimes.

A reliability check of the mobility measurement in SCLC technique can be carried out by calculating threshold voltage (V_T); voltage at which J-V curve changes from Ohmic region to quadratic region. By combining above two equations [equation (a) and equation (b)] the expression for V_T for two regimes is

$$V_T = \frac{8}{9} en \frac{d^2}{\varepsilon\varepsilon_0} \qquad \text{(c)}$$

The measured value of the mobility can be used in equation (a) to obtain *n* which, in turn, can be used in equation (c) to obtain V_T. A good match between such calculated value of V_T and the experimental value extracted from J–V curves is an indicator of reliable measurements. All measurements where the difference (calculated value of V_T and the experimental value extracted from J–V curves) was above 5% were discarded. The measurements with errors greater than 5% are actually very few.

The comparison between theoretical and experimental threshold voltage values for compound **1** (Figure S18a) and **3** (Figure S18b), exhibiting the highest hole and electron mobility values, respectively is shown below. The values are almost in perfect match with each other indicating the authenticity of the reported mobility values. The same method for validation of SCLC measurement has been reported earlier.[5,6] In addition, clean SCLC has been observed for bulk transport in solution-processed low order polymer diodes.[7]

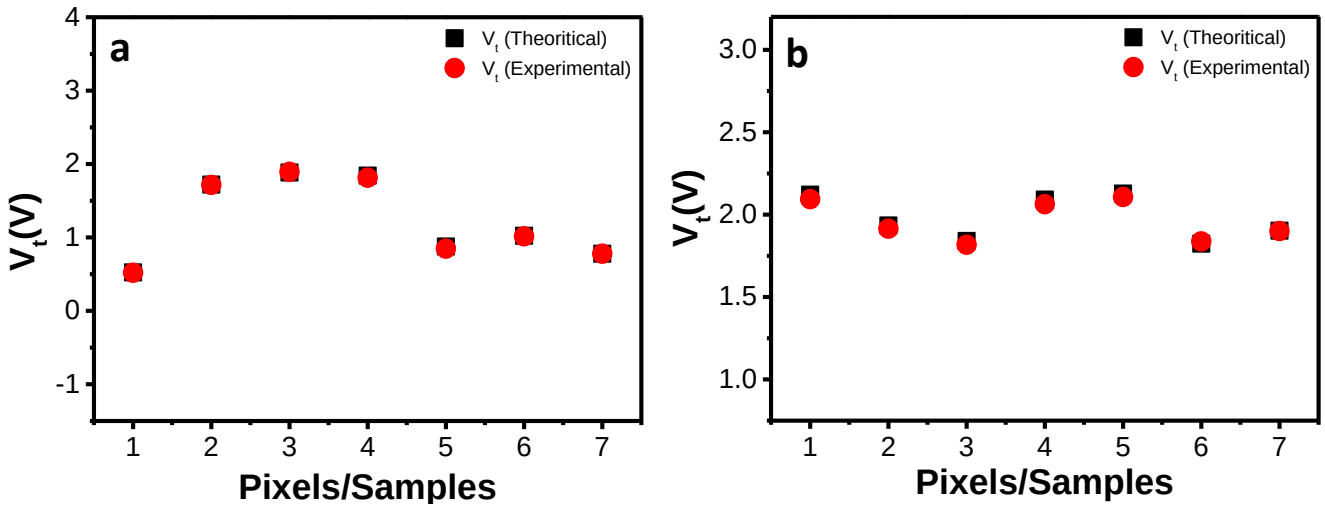

Figure S18: Comparison of theoretical and experimental threshold voltage for (a) hole mobility of **1** and (b) electron mobility of **3**.

The comparison between theoretical and experimental threshold voltage values for other compounds are also in good agreement with each other.

Thickness measurement of SCLC samples.

The thickness of prepared cells was measured by interferometry techniques using a UV-vis spectrophotometer. In this technique, one observes an interference pattern when spectrophotometer light passes through the inner walls of the sample placed perpendicular to the incident beam of the spectrophotometer, comprising of maxima and minima as shown in Figure S19. It is to be noted that if the inner walls of the cell are not nearly parallel one will not get very clear interference patterns. The thickness of the cell can be extracted using the equation

$$\boldsymbol{d} = \frac{\boldsymbol{x\lambda_1\lambda_2}}{\boldsymbol{2n(\lambda_1-\lambda_2)}} \qquad \text{(d)}$$

where d is the thickness of the cell, n is the refractive index of the air ($n \sim 1$), x is the total number of oscillation maxima between the wavelength maxima λ_1 and λ_2.

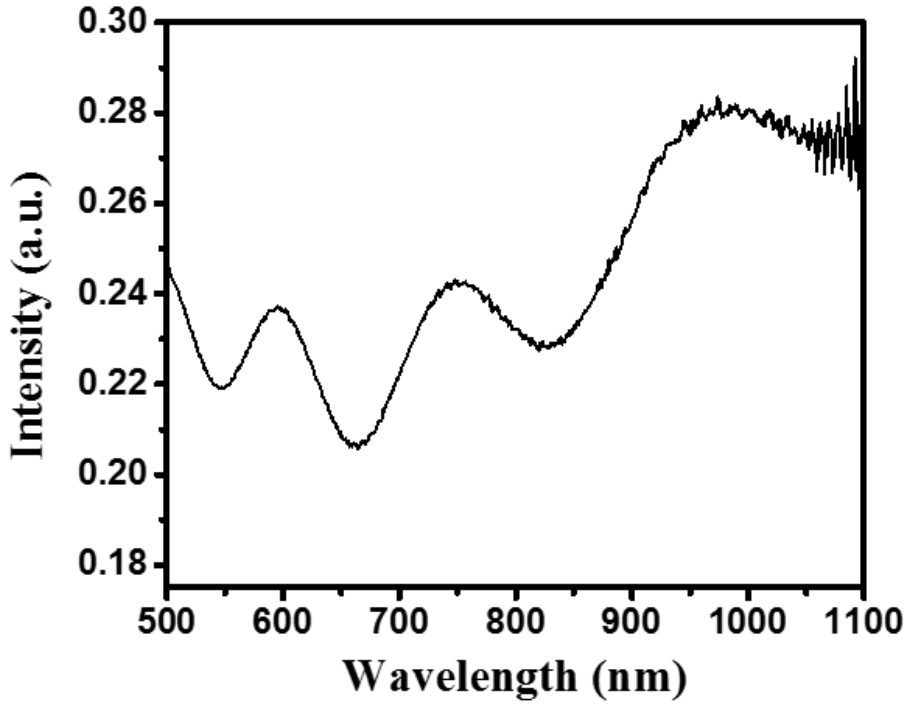

Figure S19. A typical interference pattern observed during thickness measurement for the SCLC cell in interferometric technique.

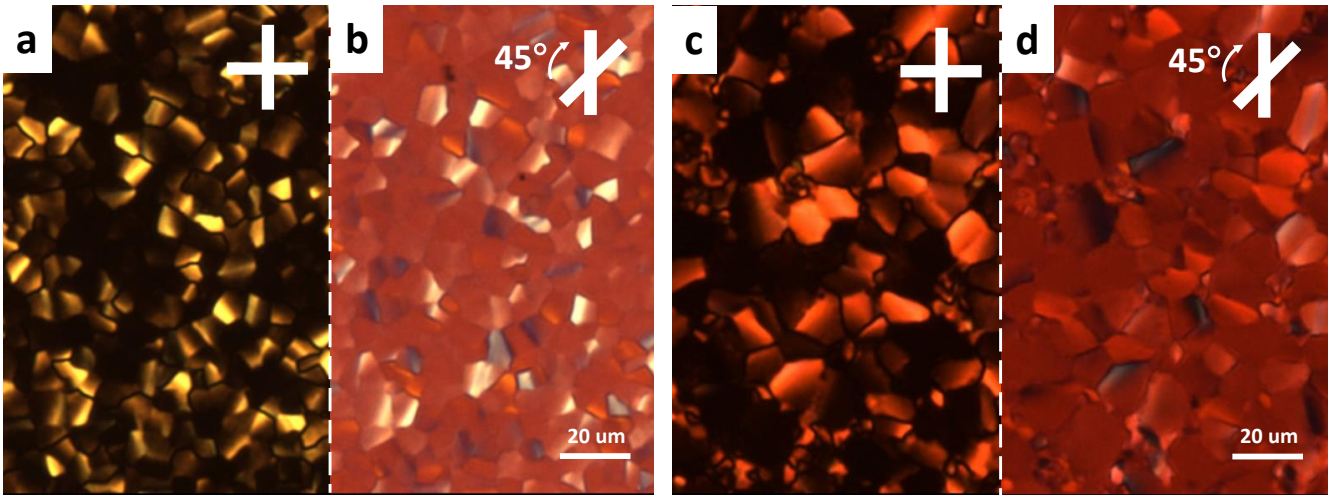

Figure S20. Optical microscopic images in hole-only cell during SCLC measurements (a, c) under crossed polarizers at 90° & (b, d) at 45° for compounds, **2** and **3**, respectively. The cell gap size for compound **2** is 3.1 µm, and compound **3** is 3.0 µm.

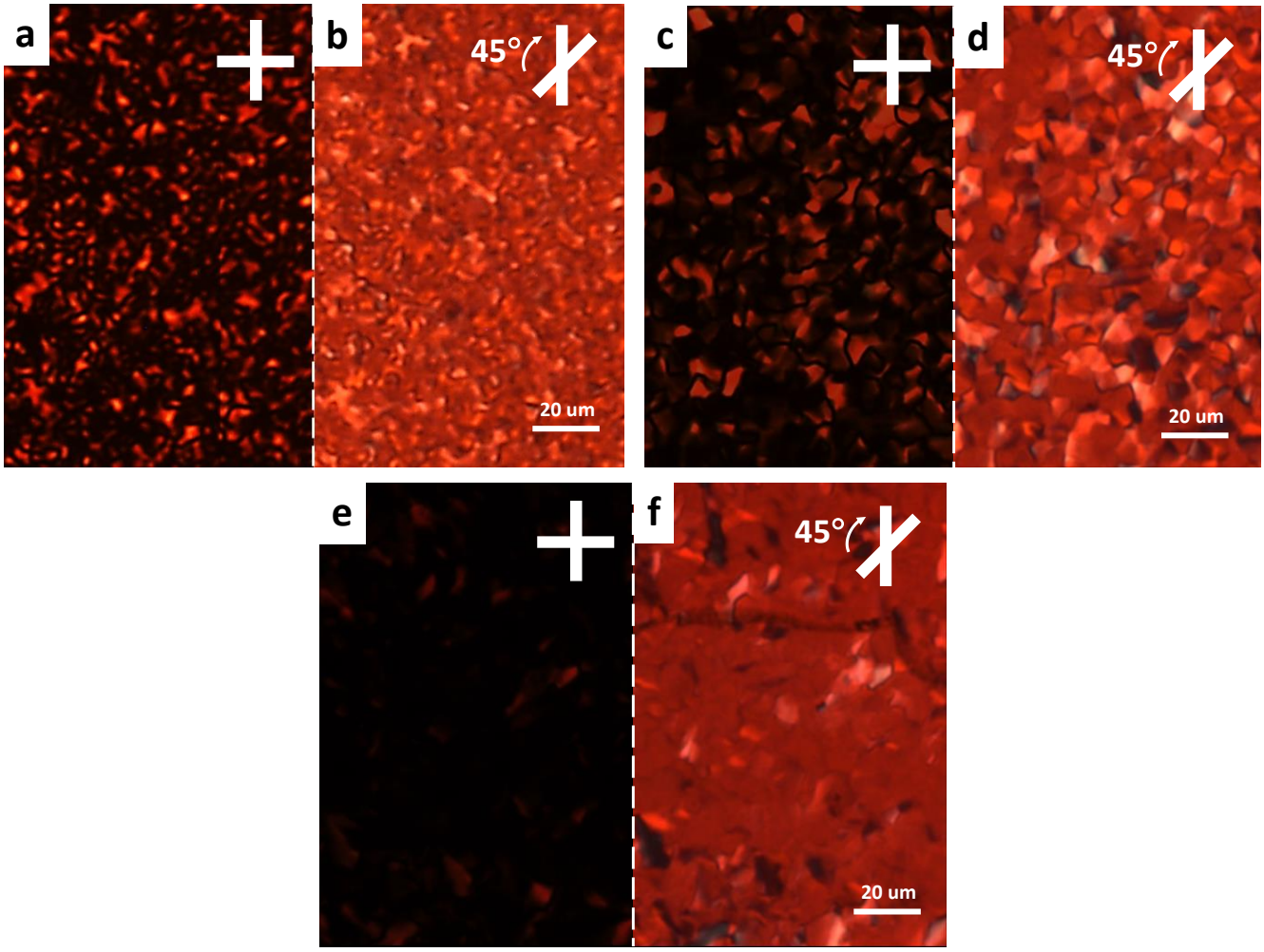

Figure S21. Optical microscopic images in electron-only cell during SCLC measurements (a, c, e) under crossed polarizers at 90° & (b, d, f) at 45° for compounds, **1**, **2** and **3**, respectively. The cell gap size for compound **1** is 4.66 µm, for compound **2** is 3.83 µm, and for compound **3** is 7.15 µm.

Table S8. Statistic table of all the mobility data of compound **1-3**[a].

Compound 1 (Hole Mobility)	**Compound 1 (Electron Mobility)**	**Compound 2 (Hole Mobility)**	**Compound 2 (Electron Mobility)**	**Compound 3 (Hole Mobility)**	**Compound 3 (Electron Mobility)**
8.8434	-	0.3627	0.3632	0.7076	2.2299
6.7397	-	0.3867	0.2137	0.3712	2.1631
7.7647	-	0.3707	0.2236	0.3914	2.0678
7.7596	-	0.3543	0.2111	0.4032	1.9579
7.9825	-	0.3210	0.2313		2.0266
	-		0.2533		3.5943
	-				3.4908
Avg = 7.81		Avg = 0.35	Avg = 0.24	Avg = 0.46	Avg = 2.50
(STD DEV = 0.75)		(STD DEV = 0.02)	(STD DEV = 0.06)	(STD DEV = 0.16)	(STD DEV = 0.71)

[a]All mobility values are in $cm^2/V.s$; Avg. value of mobility and Std. Dev. is approximated to two decimal points

Table S9. Previous literature reports of SCLC charge carrier mobility of DLC materials.

S. No.	Journals	Hole Mobility (μ_h) ($cm^2/V.s$)	Electron Mobility (μ_e) ($cm^2/V.s$)
1.	*J. Am. Chem. Soc.* **2016**, *138*, 12511-12518	$(1 \pm 0.3) \times 10^{-2}$	$(6 \pm 3) \times 10^{-3}$
2.	*Chem. Mater.* **2013**, *25*, 117-121	(2.8 ± 1.6)	-
3.	*Angew. Chem. Int. Ed.* **2011**, *50*, 7399-7402	1.4	-
4	*Adv. Mater.* **2005**, *17*, 2580-2583	-	1.3
5.	*Angew. Chem. Int. Ed.* **2017**, 129, 1279-1283	1.1	-
6.	*Chem. Eur. J.* **2018**, *24*, 3576-3583	(1.0 ± 0.5)	-
7.	J. *Mater. Chem.* **2012**, *22*, 13180-13186	0.69	-
8.	*ACS Appl. Mater. Interfaces* **2016**, *8*, 26964-26971	(0.65 ± 0.15)	-
9.	*ACS Macro Lett.* **2018**, *7*, 1138-1143	0.5	-
10.	*J. Mater. Chem. C* **2019**,*7*, 2911-2918	(0.15 ± 0.05)	-
11.	*Chem. Mater.* **2008,** *20*, 6589–6591	(0.09 ± 0.02)	-
12.	*ACS Appl. Mater. Interfaces* **2013**, *5*, 11935-11943	$(8.5 \pm 0.1) \times 10^{-3}$	-
13.	*J. Mater. Chem. C* **2014**, *2*, 7180-7183	8.72×10^{-2}	-
14.	*Chem. Eur. J.* **2018**, *24*, 17459-17463	$(4 \pm 0.7) \times 10^{-2}$	-

References

1. (a) De, J.; Gupta, S. P.; Bala, I.; Kumar, S.; Pal, S. K. *Langmuir* **2017**, *33*, 13849-13860. (b) Bala, I.; Gupta, S. P.; De, J.; Pal, S. K. *Chem. Eur. J.* **2017**, *23*, 12767-12778. (c) Bala, I.; Singh, H.; Battula, V. R.; Gupta, S. P.; De, J.; Kumar, S.; Kailasam, K.; Pal, S. K. *Chem. Eur. J.* **2017**, *23*, 14718-14722. (d) De, J.; Gupta, S. P.; Sudheendran Swayamprabha, S.; Dubey, D. K.; Bala, I.; Sarkar, I.; Dey, G.; Jou, J.-H.; Ghosh, S.; Pal, S. K. *J. Phys. Chem. C* **2018**, *122*, 23659-23674. (e) De, J.; Yang, W. Y.; Bala, I.; Gupta, S. P.; Yadav, R. A. K.; Dubey, D. K.; Chowdhury, A.; Jou, J. H.; Pal, S. K. *ACS Appl. Mater. Interfaces* **2019**, *11*, 8291-8300.

2. Bhalla, V.; Singh, H.; Kumar, M.; Prasad, S. K. Triazole-Modified Triphenylene Derivative: Self-Assembly and Sensing Applications. *Langmuir* **2011**, *27*, 15275-15281.

3. Frisch, M. J.; Trucks, G. W.; Schlegel, H. B.; Scuseria, G. E.; Robb, M. A.; Cheeseman, J. R.; Scalmani, G.; Barone, V.; Mennucci, B.; Petersson, G. A.; Nakatsuji, H.; Caricato, M.; Li, X.; Hratchian, H. P.; Izmaylov, A. F.; Bloino, J.; Zheng, G.; Sonnenberg, J. L.; Hada, M.; Ehara, M.; Toyota, K.; Fukuda, R.; Hasegawa, J.; Ishida, M.; Nakajima, T.; Honda, Y.; Kitao, O.; Nakai, H.; Vreven, T.; Montgomery, Jr. J. A.; Peralta, J. E.; Ogliaro, F.; Bearpark, M.; Heyd, J. J.; Brothers, E.; Kudin, K. N.; Staroverov, V. N.; Kobayashi, R.; Normand, J.; Raghavachari, K.; Rendell, A.; Burant, J. C.; Iyengar, S. S.; Tomasi, J.; Cossi, M.; Rega, N.; Millam, M. J.; Klene, M.; Knox, J. E.; Cross, J. B.; Bakken, V.; Adamo, C.; Jaramillo, J.; Gomperts, R.;

Stratmann, R. E.; Yazyev, O.; Austin, A. J.; Cammi, R.; Pomelli, C.; Ochterski, J. W.; Martin, R. L.; Morokuma, K.; Zakrzewski, V. G.; Voth, G. A.; Salvador, P.; Dan-nenberg, J. J.; Dapprich, S.; Daniels, A. D.; Farkas, Ö.; Foresman, J. B.; Ortiz, J. V.; Cioslowski, J.; Fox, D. J. Gaussian 09 (Revision C.01) Gaussian, Inc., Wallingford CT, **2010.**

4. Becke, A. D. Density-functional thermochemistry. III. The role of exact exchange. *J. Chem. Phys.* **1993**, *98*, 5648-5652.

5. Feringan, B.; Romero, P.; Serrano,J. L.; Folcia, C. L.; Etxebarria, J.; Ortega, J.; Termine, R.; Golemme, A.; Gimenez, R.; Sierra,T. *J. Am. Chem. Soc.* **2016**, *138*, 12511-12518.

6. García-Frutos, E. M.; Pandey, U. K.; Termine, R.; Omenat, A.; Barberá, J.; Serrano, J. L.; Golemme, A.; Gómez-Lor, B. High Charge Mobility in Discotic Liquid-Crystalline Triindoles: Just a Core Business? *Angew. Chem. Int. Ed.* **2011**, *123*, 7537-7540.

7. Nikolka, M.; Broch, K.; Armitage, J.; Hanifi, D.; Nowack, P. J.; Venkateshvaran, D.; Sadhanala, A.; Saska, J.; Masca, M.; Jung, S. H.; Lee, J. K.; McCulloc, I.; Salleo, A.; Sirringhaus, H. High-Mobility, Trap-Free Charge Transport in Conjugated Polymer Diodes. *Nat. Commun.* **2019**, *10*, 2122.